Journal of Power Sources 239 (2013) 144–150

Contents lists available at SciVerse ScienceDirect

Journal of Power Sources

journal homepage: www.elsevier.com/locate/jpowsour

Synthesis and electrochemical performances of $(1-x)LiMnPO_4 \cdot xLi_3V_2(PO_4)_3/C$ composite cathode materials for lithium ion batteries

Laifen Qin [a,b], Yonggao Xia [a,*], Bao Qiu [a], Hailiang Cao [a], Yuanzhuang Liu [a], Zhaoping Liu [a,*]

[a] Ningbo Institute of Materials Technology & Engineering (NIMTE), Chinese Academy of Sciences, Zhejiang 315201, PR China
[b] The Faculty of Science, Ningbo University, Zhejiang 315211, PR China

HIGHLIGHTS

- A series of $(1-x)LiMnPO_4 \cdot xLi_3V_2(PO_4)_3/C$ were synthesized by solid-state method.
- The ratios of $LiMnPO_4$ to $Li_3V_2(PO_4)_3$ are correlated with the properties of samples.
- The $0.6LiMnPO_4 \cdot 0.4Li_3V_2(PO_4)_3$ exhibits the best electrochemical performance.

ARTICLE INFO

Article history:
Received 14 December 2012
Received in revised form
13 March 2013
Accepted 15 March 2013
Available online 26 March 2013

Keywords:
Lithium ion batteries
Cathode material
Lithium manganese phosphate
Lithium vanadium phosphate

ABSTRACT

A series of $(1-x)LiMnPO_4 \cdot xLi_3V_2(PO_4)_3/C$ ($x = 0, 0.1, 0.2, 0.3, 0.4, 0.5, 1$) composites cathode materials are successfully synthesized by solid-state method. The structures and properties of the composites have been studied with X-ray diffraction (XRD), scanning electron microscopy (SEM), elemental mapping, high resolution transmission electron microscopy (HRTEM), energy dispersive spectroscopy (EDS) and electrochemical measurements. XRD results reveal that the composites comprise $Li_3V_2(PO_4)_3$ phase and $LiMnPO_4$ phase with a small amount of $LiVP_2O_7$ impurity. The electrochemical measurement results show that the ratios of $LiMnPO_4$ to $Li_3V_2(PO_4)_3$ are correlated with the electrochemical performances of the composite materials. Among these composites, the $0.6LiMnPO_4 \cdot 0.4Li_3V_2(PO_4)_3$ exhibits the best electrochemical performance, it can deliver specific capacity of 154 mA h g^{-1} at 0.05 C charge–discharge rate.

1. Introduction

Olivine lithium transition-metal phosphates $LiMPO_4$ (M = Mn, Fe, Co and Ni), which are firstly reported by Padhi and Goodenough et al., have attracted much attention in the past decade [1–3]. The presence of the strong covalently-bonded PO_4^{3-} tetrahedral polyanion in the olivine structure can make a stable three-dimensional (3D) framework, thus giving rise to the excellent cycling performance and thermal stability of $LiMPO_4$ cathode materials [4]. Among these phosphates, $LiFePO_4$ has established its position as one of the most promising cathode materials for high-power–density lithium ion batteries, and it has been commercialized with near-theoretical capacity and remarkable cycle performance, achieving through reducing the particle size and carbon-coating [5–8]. Compared to $LiFePO_4$, $LiMnPO_4$ has higher Li^+ intercalation potential of 4.1 V versus Li^+/Li (3.4 V for $LiFePO_4$), and the similar theoretical capacity (171 mA h g^{-1}), providing about 20% higher energy density than $LiFePO_4$ for lithium ion batteries. Moreover, the 4.1 V intercalation potential of $LiMnPO_4$ is compatible with conventional nonaqueous organic electrolytes of lithium ion batteries.

However, some intrinsic disadvantages of $LiMnPO_4$ hinder its practical applications in lithium ion batteries. Owing to the heavy polaronic holes localized on the Mn^{3+} sites (the Jahn–Teller ion) and the interfacial strain between the $LiMnPO_4$ and $MnPO_4$ phase, $LiMnPO_4$ suffers from poor electronic conductivity ($<10^{-10}$ S cm^{-1}) and low lithium diffusivity, even much worse than those of $LiFePO_4$ [9–11]. Consequently, these drawbacks lead to its low discharge capacity, high polarization and poor rate capability. In order to enhance the electrochemical performance of $LiMnPO_4$ cathode material, approaches similar to those applied to $LiFePO_4$ have been conducted, e.g.: (i) reducing particle size and customizing the particle morphologies to accelerate the diffusion of Li^+ and increase the contact area with the conductive agent such as carbon; (ii) coating the particles with a thin carbon layer to decrease the interfacial resistance on the particles boundaries; and (iii) doping

* Corresponding authors. Tel./fax: +86 574 8668 5096.
E-mail addresses: xiayg@nimte.ac.cn (Y. Xia), liuzp@nimte.ac.cn (Z. Liu).

0378-7753/$ – see front matter © 2013 Elsevier B.V. All rights reserved.
http://dx.doi.org/10.1016/j.jpowsour.2013.03.063

metal cations in the lattice of $LiMnPO_4$ to improve the lithium diffusivity and ionic conductivity [12–21].

Recently, $LiFePO_4$-based compounds with additive vanadium have been reported, which is considered as a novel strategy for improving the electrochemical performance of $LiFePO_4$ [22–39]. As another kind of promising cathode material, the monoclinic $Li_3V_2(PO_4)_3$ shows much faster lithium-ion migration rate due to its open 3D framework. Moreover, $Li_3V_2(PO_4)_3$ exhibits four redox plateaus around 3.62, 3.68, 4.08, and 4.55 V. It can extract/insert two Li ions reversibly between 3.0 and 4.3 V based on the V^{3+}/V^{4+} redox couple; three Li ions may be extracted completely when charged to 4.8 V [40,41]. To date, a series of $xLiFePO_4 \cdot yLi_3V_2(PO_4)_3$ composites have been prepared by approaches including the chemical reduction and lithiation method [28,33], solid-state reaction [22,23,30], solution method [24], so-gel [25,26,32] and rheological phase reaction [27,29]. All of the experimental results indicate that the $Li_3V_2(PO_4)_3$ additive can significantly improve the electrochemical performances of $LiFePO_4$ cathode materials. In addition, vanadium additions for $LiMn_2O_4$ and $LiCoPO_4$ have been also reported [42,43]. For example, Wang et al. [43] reported that the addition of vanadium into $LiCoPO_4$ remarkably enhances charge and discharge behavior. $Li_{1.025}Co_{0.95}V_{0.05}(PO_4)_{1.025}$/C electrode shows the first discharge capacity of 134.8 mA h g^{-1} at 0.1 C rate, higher than that of the pristine $LiCoPO_4$/C of 112.2 mA h g^{-1}, and also exhibits much better cyclic stability. Furthermore, Yang et al. [19] substituted minor Mn^{2+} by V^{3+} to synthesize $LiMn_{0.95}V_{0.05}PO_4$, and that $LiMn_{0.95}V_{0.05}PO_4$ exhibited the discharge capacity of 61 mA h g^{-1} at 2.7–4.4 V cut-off voltage at 25 °C; which is about 30 mA h g^{-1} higher than that of pure $LiMnPO_4$. Therefore, it is reasonable to believe that the V doping into the host lattice of lithium transition-metal phosphates or forming composites is an effective method for improving the electrochemical performance. We expect that $LiMnPO_4/Li_3V_2(PO_4)_3$ composites cathode materials would achieve better electrochemical performance.

With the aim to improve the electrochemical performance of $LiMnPO_4$ cathode materials, we attempted to prepare a series of $(1-x)LiMnPO_4 \cdot xLi_3V_2(PO_4)_3$/C [$(1-x)$LMP·$x$LVP/C] composites through solid-state method. In the preparation process, glucose was used as carbon source and reduction agent. The effect of different amounts of LVP additives on the properties of LMP-based compounds was investigated in detail in this paper.

2. Experimental

2.1. Preparation

Stoichiometric $CH_3COOLi \cdot 2H_2O$, $NH_4H_2PO_4$, $(CH_3COO)_2Mn \cdot 4H_2O$, NH_4VO_3 and glucose (10 wt% of the product mass) were used as starting materials. These materials were mixed in appropriate ethanol, and then ground for 6 h in a planetary ball mill under the rotation speed of 350 rpm. After that, the mixture (as precursor) was dried at 80 °C to evaporate the ethanol, then the precursor was collected and calcined at 600 °C for 4 h in argon atmosphere with a heating rate of 5 °C min^{-1}; it was sintered to obtain $(1-x)$LMP·xLVP/C ($x = 0, 0.1, 0.2, 0.3, 0.4, 0.5, 1$) composites. For comparison, the $(1-x)$LMP + xLVP/C mixture with $x = 0.4$ was prepared through mixing 60% LMP/C with 40% LVP/C.

2.2. Structure and morphology characterization

The crystalline structures of the products were characterized by X-ray powder diffraction (XRD, D8 Advance diffractometer with Cu Kα radiation). The morphologies and microstructures were observed by field emission scanning electron microscopy (SEM) (S-4800, Hitachi) and high-resolution transmission electron microscopy (HRTEM) (Tecnai F20, FEI) equipped with energy dispersive spectrometry (EDS). Elemental mapping and EDS were used to demonstrate the existence and distribution of vanadium and manganese. The amount of C was measured by using CHNS/O Elemental Analyzer (PE2400II, Perkin–Elmer).

2.3. Electrochemical measurements

Electrochemical properties of the $(1-x)$LMP·xLVP/C ($x = 0, 0.1, 0.2, 0.3, 0.4, 0.5, 1$) electrodes were studied through electrochemical cells assembled in an argon glove box. Firstly, the paste was prepared by mixing active material and Super P carbon (SP) with poly(vinylidene fluoride) (PVDF) in *N*-methyl-2 pyrrolidinone (NMP) solution. The weight ratio of active material:SP:PVDF was 80:15:5; then the paste was coated on an Al foil using automatic film-coating equipment, and dried at 120 °C for 12 h in vacuum; after that, the resultant film was punched onto 13-mm diameter discs as cathode; lastly, the coin cells were assembled in an argon-filled glove box using Celgard 2502 as separator and lithium foil as anode. 1 M $LiPF_6$ (dissolved in ethylene carbonate and dimethyl carbonate with a 1:1 volume ratio) was employed as electrolyte. The coin-type cells were tested within a voltage range of 2.0–4.5 V using a constant-current–constant-voltage (CC–CV) protocol at various rates with potentiostatic steps at the cutoff potential on a cell testing system (LAND CT2001A, China). All the tests were conducted at constant temperature (25 °C). The cyclic voltammogram (CV) was performed between 2.0 V and 4.5 V using the Solartron 1400 cell test system with a scan rate of 0.05 mV s^{-1}. All the specific capacity was determined without subtracting the mass of carbon added in synthesis of $(1-x)$LMP·xLVP/C ($x = 0, 0.1, 0.2, 0.3, 0.4, 0.5, 1$) composites.

3. Results and discussion

Fig. 1 shows the XRD patterns of the as-prepared $(1-x)$LMP·xLVP/C ($x = 0, 0.1, 0.2, 0.3, 0.4, 0.5, 1$) samples and the $(1-x)$LMP + xLVP/C mixture with $x = 0.4$. For the pattern with $x = 0$, all the diffraction peaks correspond well to the orthorhombic LMP phase with Pnmb space group (ICSD #25834). When $x = 0.1, 0.2, 0.3, 0.4, 0.5$, both the peaks of orthorhombic LMP and monoclinic LVP (space group $P2_1/n$, ICSD #96962) appear in the XRD patterns of the as-prepared materials. There is a noticeable difference in the

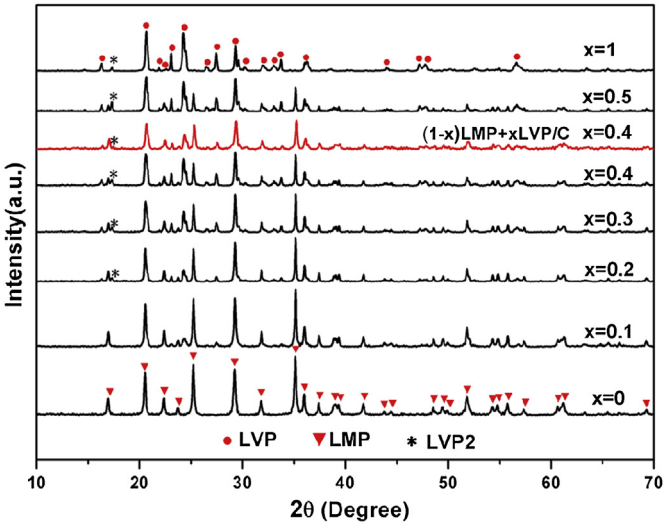

Fig. 1. XRD patterns of the prepared $(1-x)$ LMP·xLVP/C composites and the $(1-x)$ LMP + xLVP/C mixture with $x = 0.4$.

Table 1
The lattice parameters of LMP in the $(1-x)$LMP·xLVP/C ($x = 0$, 0.1, 0.2, 0.3, 0.4, 0.5) samples and carbon content.

Sample	Lattice parameters				Phase content (wt%)	*Rw* (%)	Carbon content (%)
	a (Å)	*b* (Å)	*c* (Å)	*V* (Å^3)			
$x = 0$	6.1071	10.4529	4.7473	303.0529	100 ± 0.00	5.919	2.76
$x = 0.1$	6.1039	10.4466	4.7480	302.7562	85.94 ± 1.30(LVP:12.99 ± 0.69; LVP2:1.07 ± 0.0)	4.744	2.5
$x = 0.2$	6.1020	10.4446	4.7459	302.4702	65.04 ± 1.90(LVP:27.87 ± 1.01; LVP2:7.09 ± 0.0)	4.614	1.76
$x = 0.3$	6.1019	10.4448	4.7454	302.4392	48.80 ± 1.20(LVP:42.96 ± 1.29; LVP2:8.24 ± 0.0)	4.548	1.65
$x = 0.4$	6.1017	10.4451	4.7453	302.4316	36.90 ± 1.05(LVP:54.30 ± 1.07; LVP2:8.80 ± 0.0)	5.011	1.53
$x = 0.5$	6.1011	10.4446	4.7451	302.3746	26.86 ± 1.62(LVP:63.24 ± 0.84; LVP2:9.89 ± 0.0)	4.450	1.12

characteristic peaks as the ratios of the two materials change. The diffraction peak intensity of LVP would gradually become stronger with increasing the content of LVP additives. However, for the samples with high LVP additives content ($x = 0.2$, 0.3, 0.4, 0.5, 1), a few impurities are also observed, which could be indexed with a monoclinic $LiVP_2O_7$ (LVP2) phase (ICSD #80551). Furthermore, it is worth noting that the diffraction peaks of the 0.6LMP + 0.4LVP/C mixture in red line shifts ($\sim 0.13^\circ$) to the higher angle compared to that of the 0.6LMP·0.4LVP/C composite. There is no obvious diffraction peak of carbon in all the samples, indicating that the coated carbon is amorphous or the amounts of carbon is too less to be measured. So the carbon contents of the as-prepared samples were tested by total organic carbon analysis and listed in Table 1. The carbon content decreases with the increase of the LVP amount, it is suggested that the pyrolytic carbon was increasingly consumed for the reduction of V^{5+} to V^{3+} during the preparation process.

Rietveld method was used to refine the X-ray diffraction patterns aiming to analyze the crystal structures and phase contents of the materials, and the refined results are shown in Table 1. The observed XRD patterns well match with the calculated patterns, and the reliability factors (*Rw*) are good. As shown in Table 1, the lattice volume values of LMP in the composites decrease as the contents of LVP additives increase. The changes in lattice parameters prove that some V ions have been doped into the crystal structure of LMP, because the ionic radius of V^{3+} is smaller than that of Mn^{2+}. Similar results have also been reported by Zhang et al. [23]. Meanwhile, we also believe that some Mn ions could dope into the crystal structure of LVP. From Table 1, it can be seen that the calculated weight percent of LMP and LVP phases for the samples deviates little from the theoretical value, which is attributed to the mutual doping between the two materials. It turns out that small amounts of Mn and V are doped into the lattice of LVP and LMP, respectively, and the most of Mn and V in the pristine materials tend to form the LMP and LVP phases when the doping reaches the limit. In addition, the carbon coating on the particles surface not only prevents particles from aggregating, but also increases the electrical conductivity of the samples. This structure can greatly contribute to the enhancing electrochemical performances of the composites.

Elemental mappings of MnKα and VKα in Fig. 2 corresponding to the 40 mol% substituted sample micrograph indicate that LMP and LVP phases in the mixture were well dispersed and mixed.

TEM images of the composites $(1-x)$LMP·xLVP/C with $x = 0$ and 0.4 are shown in Fig. 3(a) and (b), respectively. As shown in Fig. 3(a) and (b), the prepared particles have been uniformly coated with carbon. HRTEM was used to further study the microstructure of the as-prepared composites. Fig. 3(c) and (d) is the HRTEM image of the selected regions I and II in Fig. 3(a) and (b). The LMP/C sample

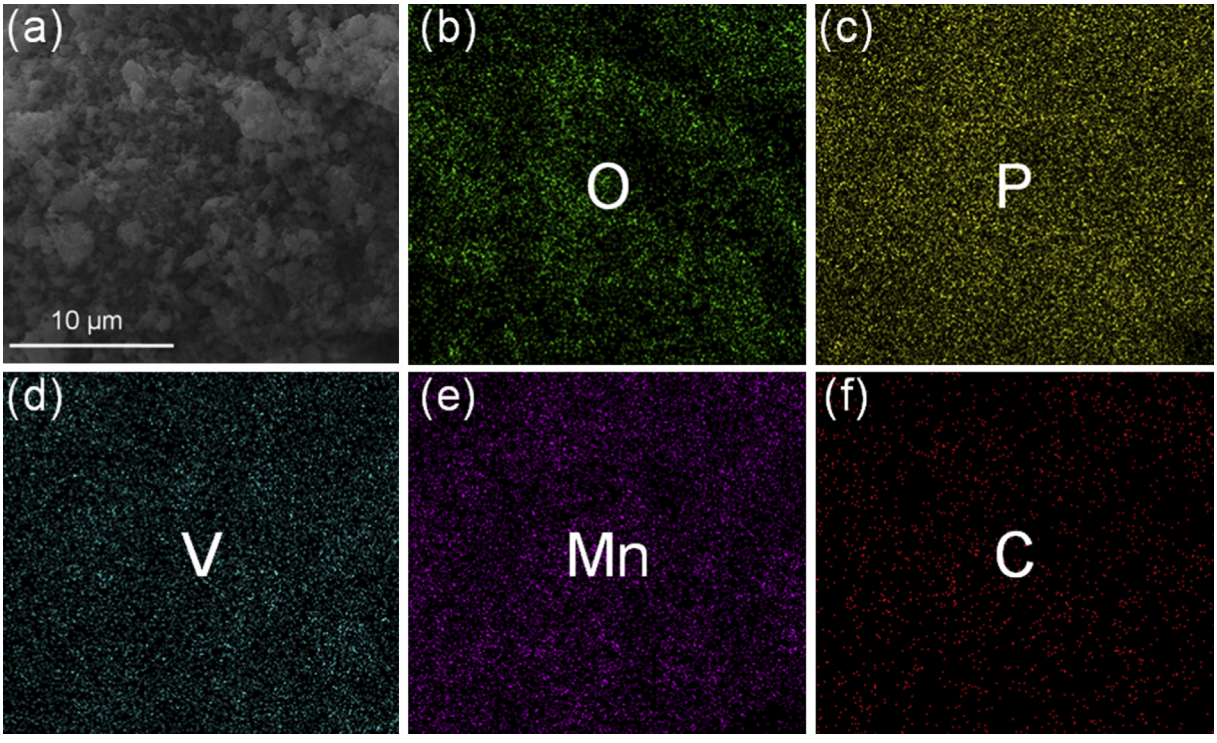

Fig. 2. SEM images of (a) xLMP·$(1-x)$LVP/C sample with $x = 0.4$ and elemental mapping for (b) O, (c) P, (d) V, (e) Mn, (f) C.

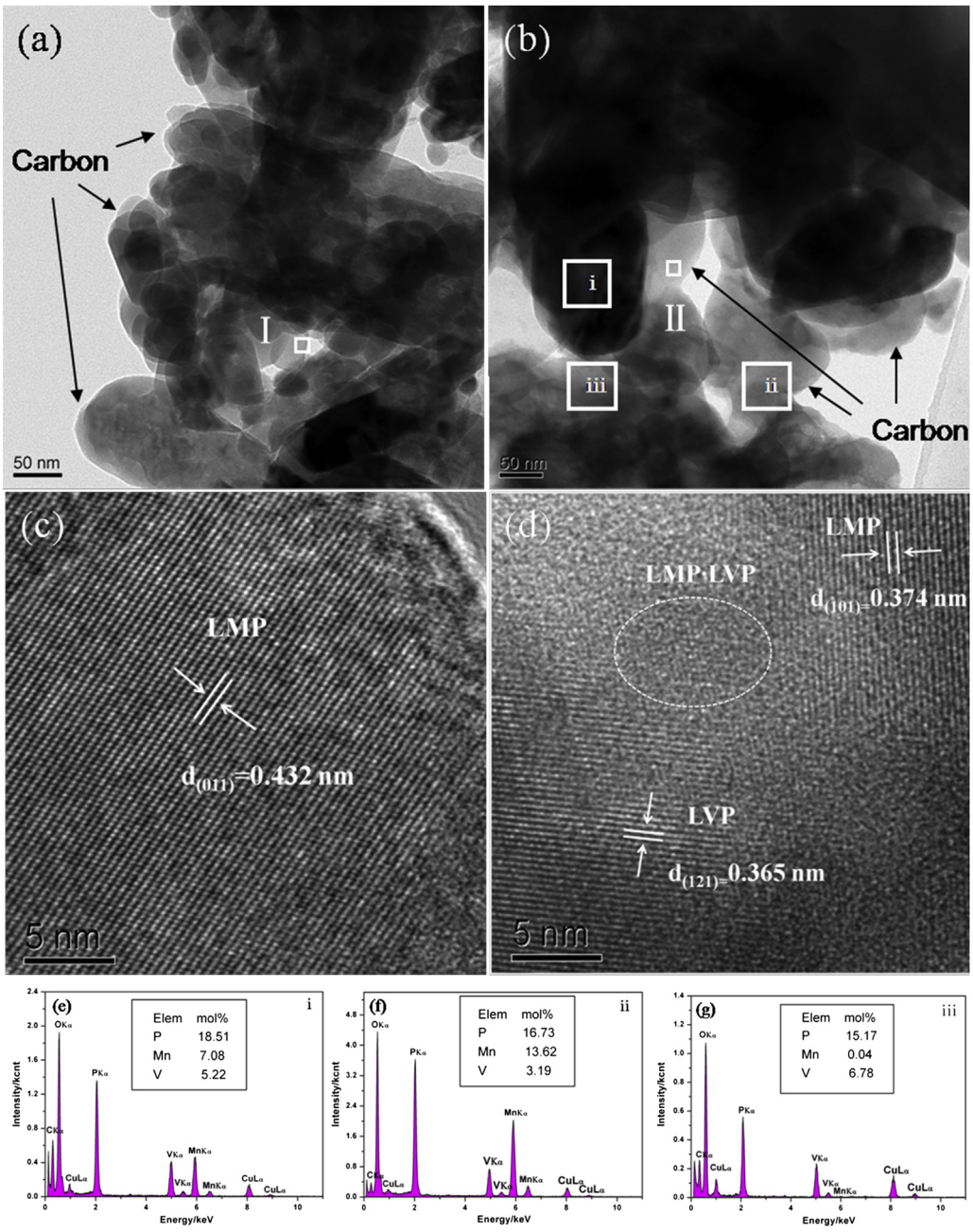

Fig. 3. TEM images of $(1-x)$LMP· xLVP/C (a) $x = 0$; (b) $x = 0.4$. HRTEM images of the selected areas (c) I (d) II. EDS spectra of regions (e) i, (f) ii, (g) iii.

exhibits regular lattice fringes of the (011) crystalline plane with measured d spacing value of 0.432 nm (ICSD #25834) in Fig. 3(c). For the $(1-x)$LMP·xLVP/C composites with $x = 0.4$, two kinds of lattice fringes in Fig. 3(d) can be seen, one is the lattice range of LMP (interplanar spacing 0.374 nm, lattice plane (101)), the other is the lattice fringe of LVP (interplanar spacing 0.365 nm, lattice plane (121), ICSD #96962). And the lattice fringes become obscure on the particle boundaries between LMP and LVP. This confirms that both LMP and LVP phases exist in the composites.

In order to deeply characterize the structure of the composites in more detail, the EDS spectra of regions i, ii and iii in Fig. 3(b) are presented in Fig. 3(e–f). All of the EDS spectra exhibit the characteristic peaks of MnKα, VKα, PKα, and OKα. There is no Li detected for the reason that the X-ray fluorescence yield is extremely low for elements such as Li or Be [26,32]. It is important to notice that the relative contents of the elements in the three regions are quite different. For region i, the molar ratio of Mn:V:P is about 7:5:18, so LMP and LVP phases should coexist in this region. For region ii, the molar ratio of Mn: P is nearly 1:1, and the amount of V is small. Nevertheless, for region iii, the molar ratio of V: P is about 2:3, and the amount of Mn is small. Obviously, regions ii and iii correspond to the V-doped LMP and Mn-doped LVP, considering the HRTEM images display single lattice fringes for LMP and LVP, respectively. Thus, it can be concluded that the partial mutual doping between LMP and LVP phases could happen during the synthetic process, which is consistent with the XRD analysis.

The initial cyclic voltammogram curves of the composites between 2.0 and 4.5 V at a scan rate of 0.05 mV s^{-1} are depicted in Fig. 4. As for the pure LMP/C ($x = 0$), there is one redox potential peaks around 4.36/3.92 V, which accords with the oxidation of

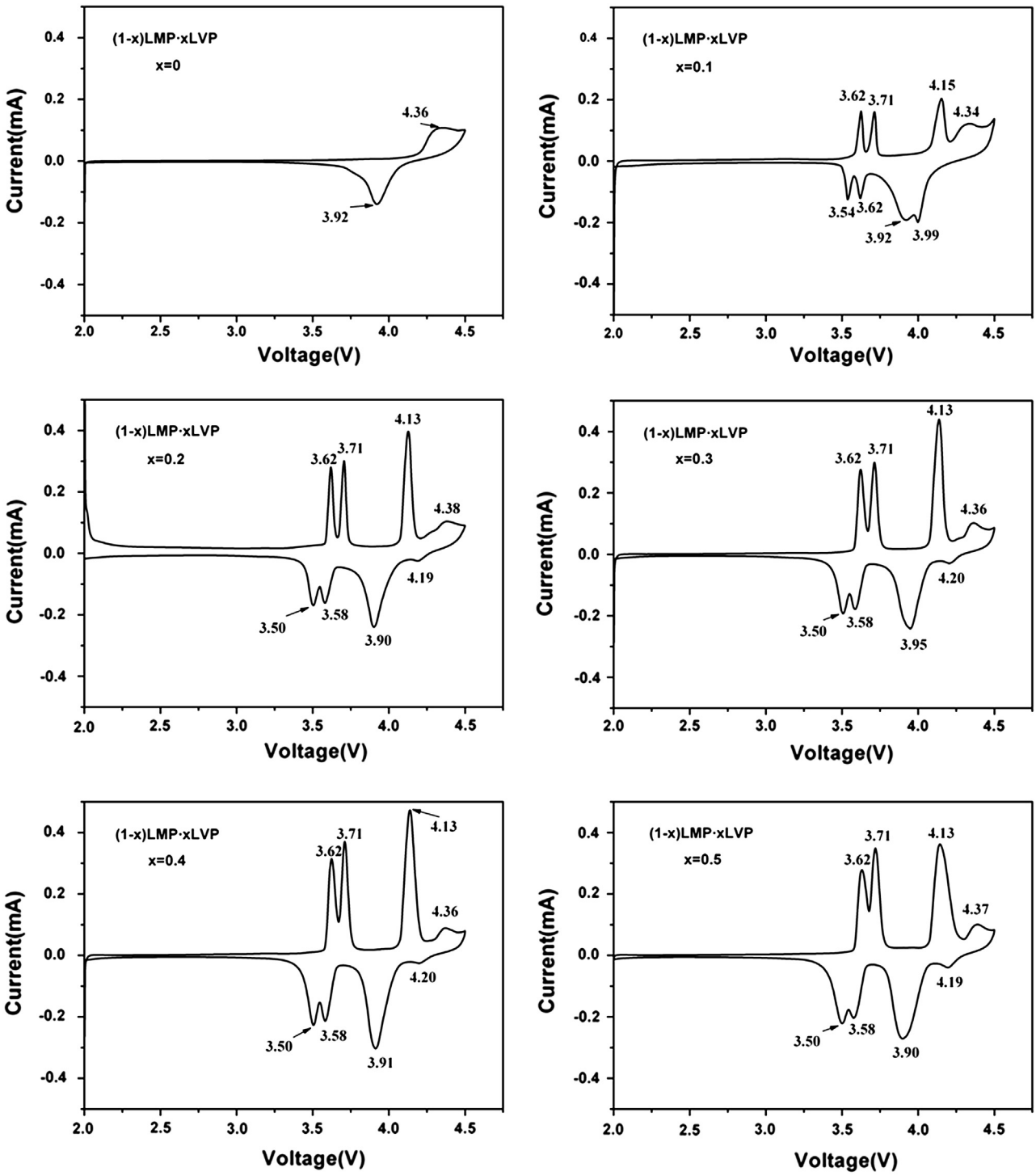

Fig. 4. Cyclic voltammetry curves of $(1-x)$LMP·xLVP/C (x = 0, 0.1, 0.2, 0.3, 0.4, 0.5).

Mn^{2+} to Mn^{3+} [44]. As far as $(1-x)$LMP·xLVP/C sample with $x = 0.1$, other three redox couple peaks of LVP (3.62/3.54, 3.71/3.62, 4.15/3.99) can be seen. Two Li^+ and a part of the third Li^+ can be cycled reversibly for $Li_3V_2(PO_4)_3$ between 2.0 and 4.5 V. The first Li^+ is removed in two steps, which is extracted around 3.6 V and 3.7 V versus Li/Li^+; the second Li^+ is extracted over one single step, 4.08 V versus Li/Li^+; a part of the third Li^+ could be extracted between 4.3 V and 4.5 V [41,45]. Accordingly, the two anodic peaks around 3.62 V and 3.71 V correspond to extract the first Li^+ via two steps; the anodic peak around 4.15 V corresponds to extract the second Li^+ via a single step. With increasing the content of LVP additives, the two cathodic peaks that belong to insert the first Li^+ from LVP shift to 3.50 V and 3.58 V, while the redox couple peaks of LMP and the third redox couple peaks of LVP appear in the way of superimposition around 4.13/3.90 V. In addition, for the LVP added samples (x = 0.2, 0.3, 0.4, 0.5), another redox potential pairs around 4.38/4.19 is observed, which could ascribe to the V^{3+}/V^{4+} redox couple peaks of LVP2. However, the cathodic or anodic peaks based on the

V^{4+}/V^{5+} redox couple which corresponds to insert or extract a part of the third Li^+ cannot be seen obviously for all the modified samples. The upward trend up to 4.5 V in the oxidation CV curves may indicate that the third Li^+ can be partially extracted. From above results, it is believed that the excessive vanadium tends to form LVP and LVP2 when the content of vanadium reaches its limit in the crystal structure of LMP. Evidently, the polarization of the Mn^{3+}/Mn^{2+} redox potential for the composites decreases comparing with the LMP/C, indicating that the composites electrodes have an improvement in the kinetics of the lithium intercalation/deintercalation at the electrode/electrolyte interface and/or the rate of lithium diffusion in the film. On the contrary, it is slightly increased for LVP due to the poor ionic electronic conductivity of LMP.

Fig. 5(a) shows the first charge–discharge curves of $(1-x)$LMP·xLVP/C ($x = 0, 0.1, 0.2, 0.3, 0.4, 0.5$) samples at 0.05 C rate from 2.0 V to 4.5 V. All the composites cathode materials behave the similar charge–discharge curves except that LMP contains one potential plateaus. Other charge curves contain four potential plateaus. The three subsequent plateaus around 3.6 V, 3.7 V, and 4.08 V belong to the extraction of Li^+ from LVP. For the LVP/C, the small plateaus around 4.3 V should be ascribed to the deintercalation of Li^+ from LVP2 and the high initial discharge capacity of 157.7 mA h g^{-1} indicates that a part of the third Li^+ must be extracted up to 4.5 V. Then another potential plateaus for the samples ($x = 0.1, 0.2, 0.3, 0.4, 0.5$) should belong to the extraction of Li^+ from LMP and small LVP2. These results are in consistent with cyclic voltammogram ananlysis. It can be clearly observed that different molar ratios of LMP and LVP in the composites lead to different electrochemical performances. As the amounts of LVP additives increase, the specific capacity of the composites increases. Among these samples, the $(1-x)$LMP·xLVP/C composite with $x = 0.4$ shows the highest discharge capacity of 154 mA h g^{-1} at 0.05 C rate. It exists the tendency of discharge capacity improvement with increasing vanadium content due to the open three-dimensional (3D) framework of the electronically conductive LVP and the doping V into the crystal structure of LMP. The discharge capacity of 150.6 mA h g^{-1} for $(1-x)$LMP·xLVP/C composites with $x = 0.5$ is similar to that of the sample with $x = 0.4$. As shown, the plateaus of LVP for the composites become longer with the decreasing of the molar ratio for LMP:LVP.

The cycling performances of all the samples are exhibited in Fig. 5(b). It was measured through charging at the rate of 0.2 C and 0.5 C for discharging. It can be seen that all the samples show excellent cycle reversible capability. The $(1-x)$LMP·xLVP/C ($x = 0.1, 0.2, 0.3$) composites cathode materials show similar discharge capacity, higher than that for LMP/C (less than 60 mA h g^{-1}). For the sample with $x = 0.4$, the initial discharge capacity is about 103.9 mA h g^{-1}, higher than that of others, closely followed by the sample with $x = 0.5$, and the discharge capacity is about 95.5 mA h g^{-1} after 50 cycles. The rate capacities were also tested by the following procedure: charge–discharge at the same rates of 0.05 C, 0.1 C and 0.2 C, and then followed by charging at 0.2 C and discharging with various rates of 0.5 C, 1 C, 2 C and 5 C. As shown in Fig. 5(c), the discharge capacities of all the modified samples apparently exceed that of LMP/C at all the rates. The $(1-x)$LMP·xLVP/C composite with $x = 0.4$ exhibits the highest discharge capacity of 125.9 and 93.8 mA h g^{-1} at 0.1 C, 1 C; whereas the LMP/C shows the lowest discharge capacity of 76.2, 61.9 mA h g^{-1}. Even at a high rate of 5 C, the discharge capacity of sample with $x = 0.4$ can still keep 74 mA h g^{-1}, which is approximate twice that of LMP/C. Moreover, the rate capacity of the 0.6LMP + 0.4LVP/C mixture was also measured. By contrast, the 0.6LMP·0.4LVP/C composite exhibits much higher discharge specific capacity at all the rates. Nevertheless, their difference is reduced as the rate is larger than 0.1 C.

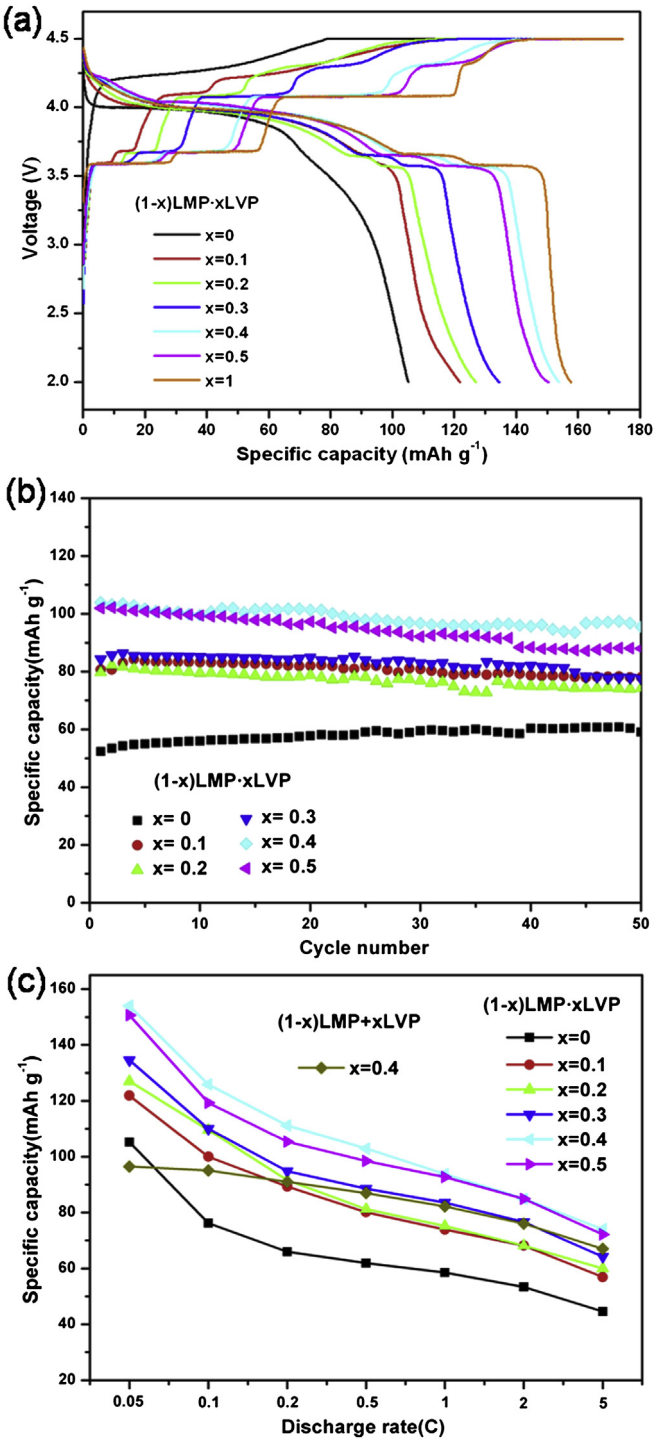

Fig. 5. (a) The first charge–discharge curves, (b) cycling performances and (c) rate capacities of the as-prepared $(1-x)$LMP·xLVP/C and the $(1-x)$LMP + xLVP/C mixture with $x = 0.4$.

4. Conclusions

A series of the $(1-x)$LMP·xLVP/C ($x = 0, 0.1, 0.2, 0.3, 0.4, 0.5, 1$) composites are prepared using $CH_3COOLi·2H_2O$, $NH_4H_2PO_4$, $(CH_3COO)_2Mn·4H_2O$, NH_4VO_3 as starting materials with glucose as the carbon source and reductive agent by solid-state method. The LMP–LVP composites contain both LMP and LVP phases with a small amount of LVP2 impurity when increasing the LVP additives ($x \geq 0.2$). It is concluded that small amounts of Mn and V as the

dopants enter into the lattice of LVP and LMP, and the most of the Mn and V in the pristine materials tend to form the LMP and LVP phases. The composites exhibit excellent electrochemical performance compared to LMP/C. Among these samples, the $(1-x)$ LMP·xLVP/C sample with $x = 0.4$ exhibits the best electrochemical performance with the discharge specific capacity of 154 mA h g^{-1} at 0.05 C, and more than 95 mA h g^{-1} at 0.5 C after 50 cycles. The outstanding performances can be ascribed to the existence of the open 3D framework of the electronically conductive LVP phase and the doping V into the crystal structure of LMP.

Acknowledgments

We are grateful for financial support from the Key Research Program of the Chinese Academy of Sciences (Grant No. KGZD-EW-202-4), the 973 program (Grant No. 2011CB935900), the Key Technology R&D Program of Ningbo (2012B10021), Ningbo Science and Technology Innovation Team (Grant No. 2012B82001).

References

[1] A.K. Padhi, K.S. Nanjundaswamy, J.B. Goodenough, J. Electrochem. Soc. 144 (1997) 1188–1194.
[2] L. Dimesso, C. Forster, W. Jaegermann, J.P. Khanderi, H. Tempel, A. Popp, J. Engstler, J.J. Schneider, A. Sarapulova, D. Mikhailova, L.A. Schmitt, S. Oswald, H. Ehrenberg, Chem. Soc. Rev. 41 (2012) 5068–5080.
[3] Z.L. Gong, Y. Yang, Energy Environ. Sci. 4 (2011) 3223–3242.
[4] C. Delmas, M. Maccario, L. Croguennec, F. Le Cras, F. Weill, Nat. Mater. 7 (2008) 665–671.
[5] X.L. Wu, L.Y. Jiang, F.F. Cao, Y.G. Guo, L.J. Wan, Adv. Mater. 21 (2009) 2710–2714.
[6] H. Song, K.T. Lee, M.G. Kim, L.F. Nazar, J. Cho, Adv. Funct. Mater. 20 (2010) 3818–3834.
[7] A. Yamada, S.C. Chung, K. Hinokuma, J. Electrochem. Soc. 148 (2001) A224–A229.
[8] H. Huang, S.C. Yin, L.F. Nazar, Electrochem, Solid-State Lett. 4 (2001) A170–A172.
[9] C. Delacourt, L. Laffont, R. Bouchet, C. Wurm, J.B. Leriche, M. Morcrette, J.M. Tarascon, C. Masquelier, J. Electrochem. Soc. 152 (2005) A913–A921.
[10] A. Yamada, Y. Kudo, K.Y. Liu, J. Electrochem. Soc. 148 (2001) A1153–A1158.
[11] N. Meethong, H.Y.S. Huang, S.A. Speakman, W.C. Carter, Y.M. Chiang, Adv. Funct. Mater. 17 (2007) 1115–1123.
[12] T. Drezen, N. Kwon, P. Bowen, I. Teerlinck, M. Isono, I. Exnar, J. Power Sources 174 (2007) 949–953.
[13] M. Pivko, M. Bele, E. Tchernychova, N.Z. Logar, R. Dominko, M. Gaberscek, Chem. Mater. 24 (2012) 1041–1047.
[14] D. Wang, H. Buqa, M. Crouzet, G. Deghenghi, T. Drezen, I. Exnar, N. Kwon, J.H. Miners, L. Poletto, M. Grätzel, J. Power Sources 189 (2009) 624–628.
[15] P.R. Kumar, M. Venkateswarlu, M. Misra, A.K. Mohanty, N. Satyanarayana, J. Electrochem. Soc. 158 (2011) A227–A230.
[16] S. Oh, S. Oh, C. Yoon, B. Scrosati, K. Amine, Y. Sun, Adv. Funct. Mater. 20 (2010) 3260–3265.
[17] Y. Sun, S. Oh, H. Park, B. Scrosati, Adv. Mater. 23 (2011) 5050–5054.
[18] T. Shiratsuchi, S. Okada, T. Doi, J. Yamaki, Electrochim. Acta 54 (2009) 3145–3151.
[19] G. Yang, H. Ni, H. Liu, P. Gao, H. Ji, S. Roy, J. Pinto, X. Jiang, J. Power Sources 196 (2011) 4747–4755.
[20] Z. Bakenov, I. Taniguchi, J. Power Sources 195 (2010) 7445–7451.
[21] T.N.L. Doan, I. Taniguchi, J. Power Sources 196 (2011) 1399–1408.
[22] F. Omenya, N.A. Chernova, S. Upreti, P.Y. Zavalij, K. Nam, X. Yang, M.S. Whittingham, Chem. Mater. 23 (2011) 4733–4740.
[23] L. Zhang, G. Liang, A. Ignatov, M.C. Croft, X. Xiong, I. Hung, Y. Huang, X. Hu, W. Zhang, Y. Peng, J. Phys. Chem. C 115 (2011) 13520–13527.
[24] M. Yang, W. Ke, S. Wu, J. Power Sources 165 (2007) 646–650.
[25] H. Tang, X. Guo, B. Zhong, H. Liu, Y. Tang, R. Xu, L. Li, J. Solid State Electrochem. 16 (2012) 1537–1543.
[26] S. Zhong, L. Wu, J. Liu, Electrochim. Acta 74 (2012) 8–15.
[27] S. Zhong, W. Chen, L. Wu, J. Liu, Ionics 18 (2012) 523–527.
[28] J. Zheng, X. Li, Z. Wang, S. Niu, D. Liu, L. Wu, L. Li, J. Li, H. Guo, J. Power Sources 195 (2010) 2935–2938.
[29] L. Wang, Z. Li, H. Xu, K. Zhang, J. Phys. Chem. C 112 (2008) 308–312.
[30] J.Y. Xiang, J.P. Tu, L. Zhang, X.L. Wang, Y. Zhou, Y.Q. Qiao, Y. Lu, J. Power Sources 195 (2010) 8331–8335.
[31] S. Zhong, L. Wu, J. Zheng, J. Liu, Powder Technol. 219 (2012) 45–48.
[32] X. Zhang, H. Guo, X. Li, Z. Wang, L. Wu, Solid State Ionics 212 (2012) 106–111.
[33] J. Zheng, X. Li, Z. Wang, J. Li, L. Li, L. Wu, H. Guo, Ionics 15 (2009) 753–759.
[34] B. Zhang, J. Zheng, Z. Yang, Ionics 17 (2011) 859–862.
[35] J. Hong, X. Wang, Q. Wang, F. Omenya, N.A. Chernova, M.S. Whittingham, J. Graetz, J. Phys. Chem. C 116 (2012) 20787–20793.
[36] H. Lin, Y. Wen, C. Zhang, L. Zhang, Y. Huang, B. Shan, R. Chen, Solid State Commun. 152 (2012) 999–1003.
[37] X.J. Chen, G.S. Cao, X.B. Zhao, J.P. Tu, T.J. Zhu, J. Alloys Compd. 463 (2008) 385–389.
[38] N. Hua, C. Wang, X. Kang, T. Wumair, Y. Han, J. Alloys Compd. 503 (2010) 204–208.
[39] G. Yang, C. Jiang, X. He, J. Ying, F. Cai, Ionics 18 (2012) 59–64.
[40] Y.Q. Qiao, J.P. Tu, J.Y. Xiang, X.L. Wang, Y.J. Mai, D. Zhang, W.L. Liu, Electrochim. Acta 56 (2011) 4139–4145.
[41] X. Zhang, H. Guo, X. Li, Z. Wang, L. Wu, Electrochim. Acta 64 (2012) 65–70.
[42] A. Eftekhari, Solid State Commun. 140 (2006) 391–394.
[43] F. Wang, J. Yang, Y. NuLi, J. Wang, J. Power Sources 195 (2010) 6884–6887.
[44] K. Saravanan, V. Ramar, P. Balaya, J.J. Vittal, J. Mater.Chem. 21 (2011) 14925–14935.
[45] L. Wang, X. Jiang, X. Li, X. Pi, Y. Ren, F. Wu, Electrochim. Acta 55 (2010) 5057–5062.